AGU PUBLICATIONS

Paleoceanography

RESEARCH ARTICLE
10.1002/2014PA002630

Key Points:
- Comparison of modern and mid-Holocene coral luminescence from NE Australia
- Proven modern sensitivity to local summer monsoon rainfall and ENSO
- Weaker mid-Holocene monsoon and ENSO but more within-season flood pulses

Supporting Information:
- Readme
- Figure S1
- Figure S2
- Figure S3
- Figure S4
- Figure S5
- Figure S6
- Figure S7
- Figure S8
- Figure S9
- Table S1
- Text S1

Correspondence to:
J. M. Lough,
j.lough@aims.gov.au

Citation:
Lough, J. M., L. E. Llewellyn, S. E. Lewis, C. S. M. Turney, J. G. Palmer, C. G. Cook, and A. G. Hogg (2014), Evidence for suppressed mid-Holocene northeastern Australian monsoon variability from coral luminescence, *Paleoceanography*, *29*, 581–594, doi:10.1002/2014PA002630.

Received 18 FEB 2014
Accepted 21 MAY 2014
Accepted article online 26 MAY 2014
Published online 17 JUN 2014

Evidence for suppressed mid-Holocene northeastern Australian monsoon variability from coral luminescence

J. M. Lough[1,2], L. E. Llewellyn[1], S. E. Lewis[3], C. S. M. Turney[4], J. G. Palmer[4], C. G. Cook[5], and A. G. Hogg[6]

[1]Australian Institute of Marine Science, Townsville MC, Queensland, Australia, [2]ARC Centre of Excellence for Coral Reef Studies, Townsville MC, Queensland, Australia, [3]Catchment to Reef Research Group, TropWATER, James Cook University, Townsville, Queensland, Australia, [4]Climate Change Research Centre, School of Biological, Earth and Environmental Sciences, University of New South Wales, Kensington, New South Wales, Australia, [5]College of Life and Environmental Sciences, University of Exeter, Exeter, UK, [6]Radiocarbon Dating Laboratory, University of Waikato, Hamilton, New Zealand

Abstract Summer monsoon rainfall in northeastern (NE) Australia exhibits substantial interannual variability resulting in highly variable river flows. The occurrence and magnitude of these seasonal river flows are reliably recorded in modern inshore corals as luminescent lines. Here we present reconstructed annual river flows for two ~120 year mid-Holocene windows based on luminescence measurements from five cores obtained from three separate coral colonies. We were able to cross-date the luminescence signatures in four cores from two of the colonies, providing confidence in the derived reconstruction. Present-day NE Australian rainfall and river flow are sensitive to El Niño–Southern Oscillation (ENSO) variability, with La Niña (El Niño) events typically associated with wetter (drier) monsoon seasons. Thus, our replicated and annually resolved coral records provide valuable insights into the northern Australian summer monsoon and ENSO variability at a key period (6 ka) when greenhouse gas levels and ice sheet cover were comparable to the preindustrial period but orbital forcing was different. Average modern and mid-Holocene growth characteristics were very similar, suggesting that sea surface temperatures off NE Australia at 6 kyr were also close to present values. The reconstructed river flow record suggests, however, that the mid-Holocene Australian summer monsoon was weaker, less variable from year to year (possibly indicative of reduced ENSO variability), and characterized by more within-season flood pulses than present. In contrast to today, the delivery of moisture appears to have been dominated by eastward propagating convective coupled waves associated with the Madden-Julian Oscillation.

1. Introduction

Reliably projecting future climatic conditions depends on the ability to realistically model both the present and times in the past subjected to different climate forcings. Knowing that such paleoclimatic models are indeed realistic depends upon comparisons with paleoclimatic records [*Braconnot et al*., 2012a, 2012b]. Reconstructions from natural archives can, however, encompass, a wide spread of ages, climate interpretation, local or regional representativeness, and temporal resolution [*Wanner et al*., 2008]. The latter becomes particularly important when trying to capture the current major source of interannual climate variability, El Niño–Southern Oscillation (ENSO) events, and assessing how these could change in the future as the world continues to warm [*Collins et al*., 2010].

Here we examine interannual variability of the northeastern (NE) Australian monsoon for two absolute-dated windows in the mid-Holocene (~6 ka). At this time the primary driver of climate differences from present was orbital forcing, leading to greater summer insolation in the Northern Hemisphere extratropics and reduced summer insolation in the Southern Hemisphere extratropics [*Braconnot et al*., 2007; *Wanner et al*., 2008]. Although some climate model studies suggest a mid-Holocene enhancement of the Australian monsoon [*Liu et al*., 2004], recent multimodel studies [*Zhao and Harrison*, 2012; *Mantsis et al*., 2013] suggest a weakening. Unfortunately, few quantitative paleoclimate reconstructions are available from northern Australia for comparison with climate simulations, but qualitative paleoclimatic data imply relatively moist conditions prior to ~5 ka [*Haberle*, 2005; *Donders et al*., 2007] which may be related to a stronger summer monsoon. Several modeling studies suggest that ENSO-driven climate variability was suppressed during the mid-Holocene and that modern ENSO variability only appeared after ~5 ka [*Clement et al*., 2000; *Conroy et al*., 2008; *Zheng et al*., 2008; *Roberts et al*., 2013]. Various

sources of proxy climate information, although limited in number, spatial coverage, and of varying temporal resolution, appear to support this [*Schulmeister et al*., 2006], though the models tend to underestimate the magnitude of the reduction in variability suggested by the proxy records [*Brown et al*., 2008].

Importantly, annual and subannually resolved stable oxygen isotope records (reflecting sea surface temperature (SST) and/or salinity) from fossil Indo-Pacific corals provide evidence for ENSO variability operating over at least the past 130 ka [*Tudhope et al*., 2001]. When compared to modern conditions some coral and other paleoclimatic records imply reduced ENSO variability in the mid-Holocene [*Moy et al*., 2002; *Gagan et al*., 2004; *Cane*, 2005; *McGregor and Gagan*, 2004; *Conroy et al*., 2008; *Wanner et al*., 2008; *Koutavas and Joanides*, 2012; *Cobb et al*., 2013; *McGregor et al*., 2013]. These and other studies also suggest that ENSO variability is currently higher than in the past, though attributing this to anthropogenic forcing is confounded by the paleo-evidence for temporal variations in the magnitude of variability [*Cobb et al*., 2013]. Modeling studies also highlight multidecadal variability in ENSO amplitude with extended periods of enhanced or suppressed activity that can make it difficult to detect ENSO responses to changing climate forcings [*Wittenberg*, 2009; *Borlace et al*., 2013]. More tropical paleoclimatic records are needed to better constrain both monsoonal and ENSO activity at key periods in the past and compare with paleoclimate model simulations [*Brown et al*., 2008; *Griffiths et al*., 2009; *Mooney et al*., 2011; *Luan et al*., 2012; *Zhao and Harrison*, 2012; *Mantsis et al*., 2013].

Rainfall across northern Australia is concentrated in the summer half year associated with the seasonal southward migration of the Australasian monsoon [*McBride*, 1987]. Summer monsoonal rainfall shows large-scale coherence across NE Australia and also substantial interannual and decadal variability [*Lough*, 1991; *Verdon et al*., 2004]. Interannual rainfall variability is linked with ENSO activity with drier conditions typically related to El Niño events and wetter conditions typically associated with La Niña events [*Lough*, 1994; *Risbey et al*., 2009]. The recent 2010–2011 and 2011–2012 La Niña events, for example, resulted in substantial flooding across large parts of Queensland [*Bureau of Meteorology*, 2012]. The strength of the teleconnection between NE Australian rainfall and ENSO is modulated on decadal time scales by the Pacific Decadal Oscillation (PDO) [*Mantua et al*., 1999; *Power et al*., 1999]. The link between ENSO and NE Australian rainfall is stronger during PDO cool phases and rainfall anomalies show greater coherence across the region and higher variability compared to PDO warm phases [*Kiem et al*., 2003; *Verdon et al*., 2004; *Meinke et al*., 2005]. Intraseasonally, monsoonal rainfall activity is modulated by the Madden-Julian Oscillation (MJO) with active and suppressed convective activity and hence rainfall associated with the passage of the wavelike disturbance across northern Australia [*Risbey et al*., 2009; *Wheeler et al*., 2009; http://www.bom.gov.au/climate/mjo/#tabs=MJO-phase]. The highly seasonal and variable rainfall regime of NE Australia also results in highly seasonal and variable river flows [*Finlayson and McMahon*, 1988; *Lough*, 1994] with eastern Australian river flows being the most sensitive in the world to ENSO extremes [*Ward et al*., 2010].

Significant freshwater discharge into the nearshore waters of the Great Barrier Reef (GBR) occurs primarily during the Australian summer monsoon. The resulting freshwater flood plumes tend to not only flow northward from the river mouths as a result of prevailing winds and the Coriolis Force but are also limited to within ~20 km from land and can be up to 20 m thick [*King et al*., 2001]. Although there are 35 river catchments draining into the GBR, two thirds of the total drainage area is contributed by the Burdekin and Fitzroy River catchments alone. The occurrence and intensity of these freshwater flood plumes is reliably recorded in inshore annually banded massive coral skeletons as luminescent lines when slices are viewed under ultraviolet (UV) light [*Isdale*, 1984]. The luminescent lines are the result of terrestrial humic and fulvic acids transported in the flood plumes being incorporated into the coral skeleton [*Boto and Isdale*, 1985]. They have been shown to reflect river flow and rainfall in adjacent catchments on the GBR [*Lough et al*., 2002; *Jupiter et al*., 2008; *Lewis et al*., 2012] and other tropical coral reef sites [*Scoffin et al*., 1989, for Papua New Guinea; *Fang and Chou*, 1992; *Peng et al*., 2002; *Grove et al*., 2010]. Coral luminescence records have also been used to develop robust reconstructions of tropical river flow and rainfall over recent centuries [*Smith et al*., 1989; *Isdale et al*., 1998; *Hendy et al*., 2003; *Lough*, 2007, 2011; *Grove et al*., 2013] and to infer rainfall regimes that differ from present in the late Quaternary [*Klein et al*., 1990]. There are, however, a few reports of luminescent lines in corals which appear to have no correlation with river flow or rainfall (e.g., *Scoffin et al*. [1989] for south Thailand and *Moses and Swart* [2006] for Tobago) or where there is no immediate source of freshwater flow to the reefs (e.g., *Tudhope et al*. [1996] for southern Oman).

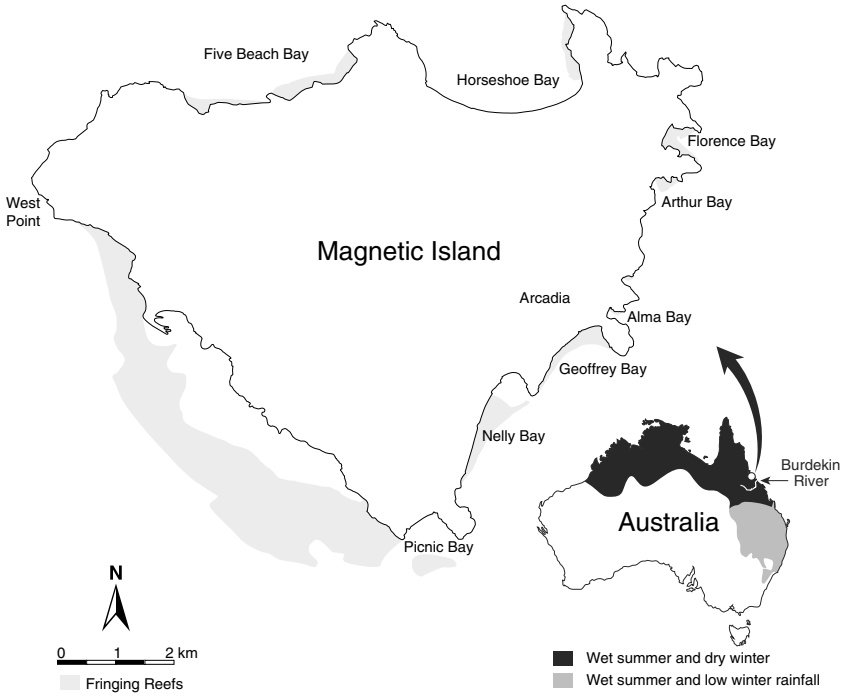

Figure 1. Map of Magnetic Island and Nelly Bay, Australia, showing occurrence of coral reefs (shading) and Nelly Bay. Inset shows seasonality of annual rainfall across northern and eastern tropical Australia (adapted from Australian Bureau of Meteorology, www.bom.gov.au) and the Burdekin River.

During dredging in 2001 for construction of a marina in Nelly Bay, Magnetic Island, central GBR (~19°S, 147°E, Figure 1), several large (2–3 m), whole massive *Porites* corals were retrieved from under ~0.5 m of sediment on the sea floor. A preliminary assessment of their age, based on their location, suggested that they lived and died in the mid-Holocene between ~4 and 7 ka—a key period for paleoclimate modeling [*Harrison et al.*, 2002]. Corals in Nelly Bay are most strongly influenced by annual freshwater flood plumes of the Burdekin River [*King et al.*, 2001] which currently enters the GBR lagoon ~100 km to the south.

Here we examine the annually resolved luminescence records in three of these mid-Holocene corals and compare them with three modern corals from the same location. We report accurate radiocarbon dating of the mid-Holocene corals, a comparison of modern and mid-Holocene humic acid signatures, assessment of diagenetic alteration of the coral skeletons, and the development of a mid-Holocene reconstruction of Burdekin River flow. Specifically, we consider whether the environment for coral growth in Nelly Bay and the signature of Burdekin River flood events, and inferred NE Australian monsoon variability, were substantially different between the mid-Holocene and the present.

2. Materials and Methods

2.1. Coral Samples

Eight mid-Holocene corals recovered from Nelly Bay in 2001 were returned to the Australian Institute of Marine Science (AIMS) and two to three cores extracted from each colony using standard drilling techniques [*Isdale and Daniel*, 1989]. When X-rayed, ~7 mm thick slices from some of the cores showed annual density banding patterns suitable for dating and extraction of growth and geochemical information [*Lough and Cooper*, 2011] and all cores showed luminescent lines when slices were viewed under UV light. Here we focus on five cores from three of these corals: two from NEL03 (NEL03A and NEL03D), two from NEL07 (NEL07B and NEL07C), and one from NEL01 (NEL01D) for which initial radiocarbon and U/Th dating indicated the corals lived and died nearly contemporaneously during the mid-Holocene ~6 ka [*Lewis*, 2005]. For comparison, three modern short cores (NEL29A, NEL35A, and NEL39B), collected from living corals in Nelly Bay in 2004, were selected from the AIMS coral core archive (Table 1). Some additional analyses were undertaken on a

Table 1. Details of Coral Cores[a]

AIMS Sample ID	Years
Mid-Holocene	
NEL03A	298 to 232
NEL03D	313 to 234
NEL07B	294 to 188
NEL07C	294 to 199
NEL01D	128–75, 67–0
Modern	
NEL29A	1952–2002
NEL35A	1971–2002
NEL39B	1972–2002

[a]Year 0 is the last dateable year at the outermost (youngest) surface of NEL01D which was ~2 cm from the colony surface. There is a 7 year gap in the NEL01D record (Years 68 to 74) associated with a growth hiatus—the length of the gap was determined from an adjacent core. Allowing for the 60 year gap identified by radiocarbon dating (section 3.1), years for cores from NEL03 and NEL07 are dated relative to Year 0 of NEL01D.

modern core from Geoffrey Bay, Magnetic Island, collected in May 1987 (AIMS ID MAG01D) previously used in the reconstruction of NE Queensland summer rainfall [*Lough*, 2011].

2.2. Radiocarbon Dating of Corals

2.2.1. Sample Pretreatment and Measurement

Contiguous decadal samples were taken for radiocarbon dating through NEL03D, NEL07B, and NEL01D pretreated at AIMS using the technique of *Nagtegaal et al.* [2012]. Samples were cleaned with analytical grade sodium hypochlorite (one part of reagent grade, 8–12.5% available chlorine to one part Milli-Q) for ~20 h to remove nonskeletal matter trapped in the corals prior to being subsampled and dated. Samples were then rinsed 3 times with Milli-Q water in an ultrasonic bath for 10 min, blown with compressed air (to remove loose particles) and dried in a 40°C oven. At the University of Waikato samples were given a light acid wash to remove any surface contamination during shipment. Coral blocks weighing 8–10 g were digested with 2 M HCl and the CO_2 subsampled for Accelerator Mass Spectrometry (AMS) analysis, with graphite produced at the University of Waikato (laboratory code "Wk") and ^{14}C analysis at the University of California at Irvine. Oxalic acid II (HOxII) was used as the normalizing standard with Carrara Marble used as the Background blank. $\delta^{13}C$ fractionation correction was achieved with measurements obtained from the AMS spectrometer itself.

2.2.2. Radiocarbon Calibration Using Marine 13 and OxCal 4.1

To calibrate the sequence of ages, we wiggle-matched the radiocarbon ages to the Marine13 curve [*Reimer et al.*, 2013] using the calibration program OxCal 4.1 [*Bronk Ramsey*, 2008; *Bronk Ramsey and Lee*, 2013; see supporting information]. The Marine13 curve was generated by a marine-atmosphere-ocean box model and represents a hypothetical "global" marine reservoir [*Reimer et al.*, 2013]. Although Marine13 provides a baseline for ocean variations in ^{14}C, a local marine reservoir age correction of 11 ± 13 years had to be applied using local preindustrial observations (http://calib.qub.ac.uk/marine/). We assumed annual precision with no counting error and used the option "Defined Sequence" (D-sequence) to fix the period (10 years) between the midpoints of the dated decadal blocks; where the two coral sequences for NEL03D and NEL07B overlap, the period between midpoints was 5 years.

Using Bayes theorem, it is possible to use prior knowledge in the calibration of radiocarbon ages to increase the accuracy and precision of the age model. In the context of the Nelly Bay corals, this prior information is the known chronological sequence of growth. The probability distribution of each radiocarbon age measurement is first treated independently of the other ages in the analysis. The calibration is then constrained to take into account coral growth. The result is a sequence of prior (unconstrained) and posterior (constrained) probability distributions, and the difference expressed as an agreement index. By adjusting the positions of the data points within their uncertainties, a record of known duration can therefore be fixed against an absolutely dated sequence (Marine13), with the posterior probability densities quantifying the most likely age distributions.

All Nelly Bay ages had a large overlap with the likelihood probability distribution and returned an agreement index >60%. The overall model agreement index was 252.3%. This high level of agreement provides confidence in the chronology and supports the use of Marine13 as a marine calibration curve for the mid-Holocene. Surprisingly, our results suggest little, if any, difference in the local marine reservoir age during the mid-Holocene. The resulting best fit against the calibration curve implies a 60 year gap between the youngest dated section of NEL07B and the oldest part of the NEL01D sequence.

2.3. Coral Growth and Luminescence Measurement and Dating

Skeletal density and luminescence were measured along each core slice using AIMS densitometer/luminometer [*Barnes et al.*, 2003; *Lough and Cooper*, 2011]. Each year of growth was identified from the X-rays and density versus distance measurements. Three annual growth variables were obtained: skeletal density, linear extension

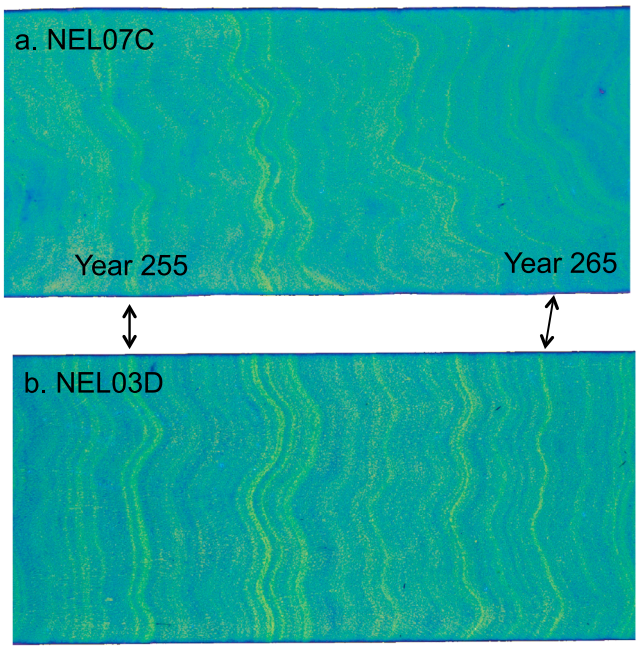

Figure 2. Digitally enhanced photographs of coral slices under UV light for (a) NEL07C and (b) NEL03D illustrating matching patterns of luminescent lines. Mid-Holocene Years 255 and 265 marked by arrows.

between adjacent density minima, and, the product of these, calcification. Similarly, three luminescence variables were obtained from photographs of coral luminescence under UV light and luminescence versus distance measurements: annual maximum, annual minimum, and annual luminescence range (the difference between summer maximum luminescence and previous winter minimum luminescence) [*Lough*, 2011]. "Monthly" luminescence values were interpolated from the luminescence versus distance measurements between adjacent luminescence minima for selected portions of the samples.

The patterns and intensity of luminescent lines in the three modern corals (NEL29A, NEL35A, and NEL39B), examined in photographs of coral slices under UV light, closely matched each other. For the mid-Holocene corals we were also able to cross-date the patterns of luminescent lines in the replicate cores from NEL03 and NEL07. Excitingly, we were then able to cross-date the luminescent lines in slices from the two separate colonies (Figure 2). This meant we could exactly match the same year in the different colonies over a 61 year period, providing a combined record extending for 126 years from the youngest dateable year of NEL07B (~2 cm from the outer edge of the core) through the oldest dateable year at the base of NEL03D. We could not match the luminescent patterns in these two colonies with NEL01D but were able to extract annual luminescence data for Years 0 to 67 and Years 75–128, relative to the last dateable year in this core which was ~2 cm from the outer edge. The 7 year gap (Years 68–74) was associated with a growth hiatus, the duration of which we were able to identify from an adjacent, but much shorter core, from the NEL01 colony.

2.4. Coral Diagenesis

Coral samples (2 × 2 cm) from the upper and lower sections of a modern coral MAG01D and the mid-Holocene corals NEL01, NEL03, and NEL07 were analyzed for secondary aragonite or calcite replacement by a JEOL JSM-5410LV Scanning Electron Microscope (SEM) at the Advanced Analytical Centre at James Cook University. Samples were platinum coated, to divert the negative charge, and placed in the SEM. Images were taken at 100 × and 2000 × magnifications and photographed. Eight thin sections were also prepared from these four cores. These samples were impregnated with a blue-dye resin, so the coral pores could be identified and discriminated from the skeleton. Samples were then glued onto frosted glass and ground down to approximately 60–100 μm. The thin sections were placed under a Leica IM50 microscope and photographed with a mounted Leica digital camera.

Table 2. Average (±1 SD) Growth and Luminescence Characteristics for Modern and Mid-Holocene Corals

Variable	Modern	Mid-Holocene
Density g cm^{-3}	1.17 ± 0.06	1.23 ± 0.13
Extension mm yr^{-1}	13.34 ± 4.43	12.14 ± 3.58
Calcification g cm^{-2} yr^{-1}	1.56 ± 0.54	1.48 ± 0.44

2.5. Comparison of Luminescence Properties of Modern and Mid-Holocene Corals

To assess whether the luminescence properties of the mid-Holocene (NEL03) and modern (NEL29) corals were similar, wavelength-defined photoluminescence images were created using the technique of *Llewellyn et al*. [2012]. Briefly, the coral surface was scanned in a matrix (0.25 × 0.25 mm spacing) measuring light caused by photoexcitation with wavelength-defined filters. Measurements were rendered using image analysis software (NIH ImageJ 1.60) where each pixel represents the photoluminescence at that *XY* location on the coral surface. Images obtained at different excitation and emission wavelength pairings were aligned to enable extraction of measurements at the same location under different conditions. This was used to produce a pseudo-excitation:emission matrix for the maximum and minimum regions of photoluminescence intensity on each coral piece. Measurements were normalized by dividing their intensity by the resolution of the excitation: emission filter (i.e., excitation filter bandwidth × emission filter bandwidth) and then standardized to the maximum intensity for the 13 filter pairs which was set to 100%.

The temperature of the measurement chamber was also varied from ambient to 45°C allowing construction of thermal quench curves by exposing corals to a range of temperatures at different combinations of excitation and emission wavelengths. The resulting quench curve slopes measure the sensitivity of coral photoluminescence to warming.

2.6. Observational Data

The modern coral data were compared to Burdekin River daily and monthly flows obtained from Queensland Department of Environment and Resource Management (www.derm.qld.gov.au), 1922–2013 and NE Queensland (~11°S–23°S, 144°E–151°E) summer (October–March) rainfall derived from the Australian Bureau of Meteorology gridded rainfall data set [*Lough*, 2011].

3. Results

3.1. Coral Ages

Radiocarbon (^{14}C) dating of contiguous decadal-length segments through NEL03D and NEL07B provided an absolutely dated chronology with a calendar age that spans 6223 to 6098 year B.P. (Table S1 and Figure S1 in the supporting information). This appears to have been followed by a 60 year gap with NEL01D dated to 6038 to 5918 year B.P. Thus, the mid-Holocene coral cores from Nelly Bay lived and died around the 6 ka period used for model comparison studies [*Mantsis et al*., 2013].

Based on this dating, we assigned Year 0 to the last dated year at the outer edge of NEL01D (i.e., 5918 year B.P.). Allowing for the 60 year gap, the youngest year of NEL07B was assigned Year 188 and the oldest year of NEL03D was assigned Year 313. Cross-dating of cores also showed that NEL07 died 44 years after NEL03. Thus, we obtained four time series of coral luminescence from two colonies (NEL03 and NEL07) which could be precisely related to each other and overlapped for 61 years (Years 294 to 234) and a single time series from colony NEL01 for Years 128 to 0.

3.2. Coral Diagenesis and Luminescence Properties

Microscopic analyses of the fossil corals (scanning electron microscopy (SEM) and thin sections) were used to determine if they were free of diagenesis. The presence of secondary aragonite or calcite replacement can strongly influence, for example, sea surface temperature (SST) reconstructions from coral geochemistry [*Enmar et al*., 2000; *Müller et al*., 2001; *McGregor and Gagan*, 2003]. The first signs of diagenesis typically occur in the basal section or toward the top of the coral and hence these areas received particular attention [*Enmar et al*., 2000; *Hendy et al*., 2007; *McGregor and Abram*, 2008].

Scanning electron microscopy (SEM) of the mid-Holocene corals showed there was no obvious addition of secondary aragonite in the coral pore spaces or on the surface of the coral slices (Figure S2). In addition, there were no other clear signs that the corals had been diagenetically altered (e.g., calcite replacement), although there was possibly some signs of dissolution features. We note, however, that the modern coral also displayed similar features (Figures S2a and S2b). The coral thin sections displayed the original internal fabric of the coral;

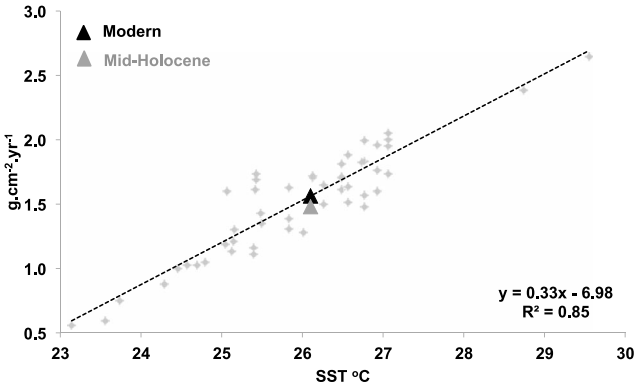

Figure 3. Average annual calcification rate versus annual average sea surface temperature for massive *Porites* from 49 Indo-Pacific sites (grey diamonds) and linear regression equation [*Lough*, 2008]. Modern Nelly Bay average calcification plotted as black triangle versus 1971 to 2000 average SST (19.5°S/147.5°E) and mid-Holocene (6.1 to 6.2 ka) average calcification rate as grey triangle.

however, they also showed what appeared to be cement surrounding some of the coral pores (Figure S3). This feature was present throughout all the corals, including the upper sections of the modern coral (Figures S3a and S3b). This possible "cement" seems likely, therefore, to be an artifact of the blue-dye impregnation procedure. Therefore, it is considered that the modern and mid-Holocene corals are free of secondary aragonite and aragonite has not been replaced with calcite.

Luminescence properties of mid-Holocene and modern corals were found to be almost indistinguishable (Figure S4). Specifically, the shape and peak of luminescence excitation-emission matrices, and the linear relationship between intensity and sensitivity to thermal quenching, at both minimum and maximum luminescence did not differ between the mid-Holocene and modern samples. This preservation of organic matter and coral luminescence in coral skeletons is also consistent with earlier studies [*Ingalls et al.*, 2003; *Klein et al.*, 1990]. We, therefore, conclude from these various lines of evidence that the skeletal properties we measured in the modern and mid-Holocene corals are comparable.

3.3. Average Coral Growth Characteristics

The often convoluted appearance of the annual density banding patterns was similar in the mid-Holocene and modern corals (Figures S5 and S6) and typical for the nearshore, turbid environment of Nelly Bay. Average skeletal density for the three mid-Holocene corals was slightly higher than modern and extension slightly lower and there was no significant difference in average annual calcification rate (Table 2). Mid-Holocene and modern Nelly Bay *Porites* growth rates were within the range of modern corals across the GBR: 12.5 ± 3.4 mm yr^{-1} (1.3–22.1) for extension, 1.30 ± 0.15 g cm^{-3} (0.92–1.93) for density and 1.60 ± 0.38 g cm^2 yr^{-1} (0.51–2.81) for calcification based on 357 colonies [*Lough et al.*, 1999]. Average massive *Porites* calcification is significantly related to average annual sea surface temperature (SST) [*Lough and Barnes*, 2000; *Lough*, 2008]. Both modern and mid-Holocene calcification rates were close to that expected based on modern average annual SST of 26.1°C at Nelly Bay (Figure 3).

3.4. Average Coral Luminescence Characteristics

Average luminescence range of both mid-Holocene coral series was significantly different from the modern series (50% and 54% of modern for NEL01D and NEL 03 and 07, respectively) but not significantly different from each other (significance at 5% level based on Student's *t* test; Figure 4). Most of this difference from modern values was due to lower luminescence maxima for the two mid-Holocene series (78% and 86% of modern for NEL01D and NEL03 and 07, respectively) compared to luminescence minima (90% and 99% of modern for NEL01D and NEL03 and 07, respectively). In the modern record, the annual minimum luminescence occurs during the dry winter months when freshwater inputs to the central GBR lagoon are minimal. The coefficient of variation (% cv) of the luminescence range was 56% in the modern record and 44% for NEL01D and 41% for NEL03 and 07, i.e., 12–15% lower interannual variability in the mid-Holocene.

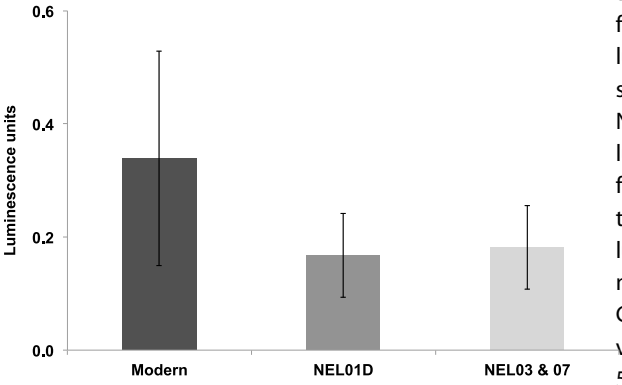

Figure 4. Mean ± standard deviation (SD) luminescence range for modern corals, NEL01D, and NEL03 and 07.

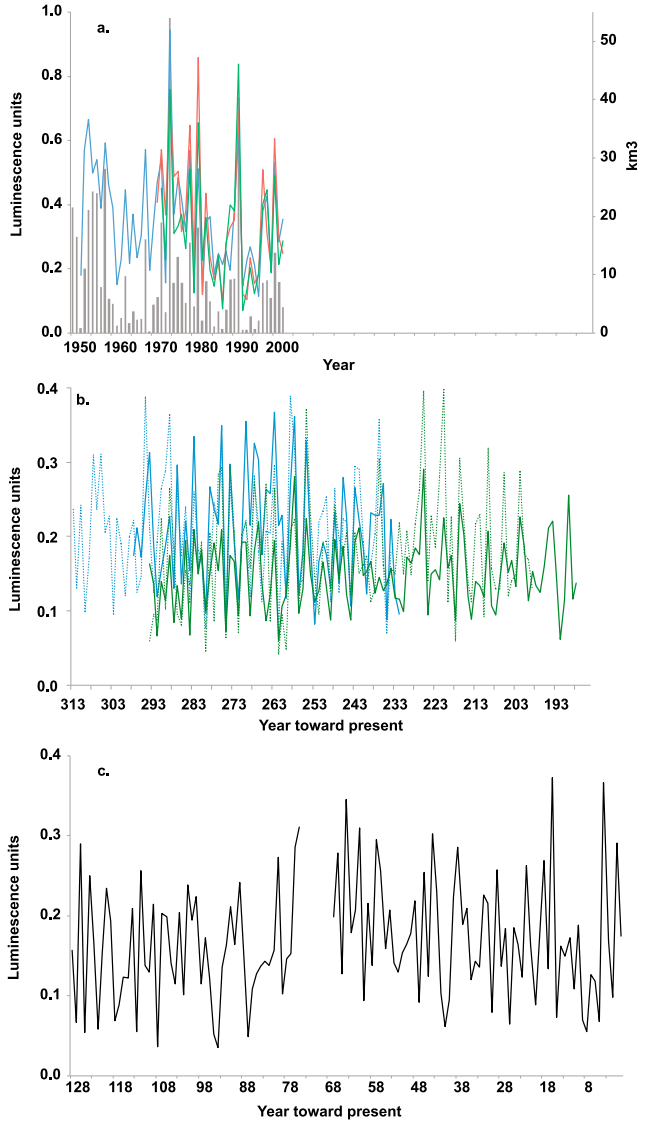

Figure 5. (a) Annual modern luminescence range series for NEL29B (blue, 1952 to 2002), NEL35A (red, 1971 to 2002), NEL39B (green, 1972 to 2002), and October–September Burdekin River flow (grey bars, 1950 to 2002); (b) annual mid-Holocene coral luminescence range series for NEL03A (blue, Years 298 to 232), NEL03D (dashed blue (Years 313 to 234), NEL07B (green, Years 294 to 188), and NEL07C (dashed green, Years 294 to 199)); and (c) annual luminescence range series for NEL01D, Years 128 to 75, 67 to 0.

3.5. Luminescence Time Series

The three modern coral luminescence series showed similar variations through time that matched those of Burdekin River flow (Figure 5a). The three series were significantly correlated with each other sharing 88–94% variance with the three-core average series. The individual and average series were significantly correlated with Burdekin River flow and NE Queensland summer rainfall (Table 3), illustrating that the annual luminescence records from modern corals in Nelly Bay are robust proxies for local river flow and the NE Australian summer monsoon [*Lough et al.*, 2002; *Lough*, 2011].

The four overlapping mid-Holocene luminescence series for the 6.2 to 6.1 ka period showed similar variations through time (Figure 5b) and were also significantly correlated over the common period Years 294 to 234 (Table 4). Individual coral time series shared between 67 and 76% variance with the four-core average series, thus confirming the visual cross-dating (Figure 2). Lead/lag correlations between the average luminescence range time series for NEL03 and NEL07 (Figure S7) again confirms the visual cross-dating and that NEL07 died

Table 3. Correlations Between Modern Luminescence Indices for Three Cores, Three-Core Average Series, Burdekin River October–September Flow, and Queensland Summer (October–March) Rainfall, 1972 to 2002 (All Values Significant at 5% Level)

	NEL29A	NEL35A	NEL39B	Three Core	Burdekin	Queensland Rainfall
NEL29A	1					
NEL35A	0.84	1				
NEL39B	0.86	0.90	1			
Three core	0.94	0.96	0.97	1		
Burdekin	0.89	0.78	0.89	0.89	1	
Queensland rainfall	0.73	0.66	0.67	0.72	0.75	1

44 years after NEL03. The slightly younger (6.0 to 5.9 ka) single coral luminescence range time series (NEL01D) is shown in Figure 5c.

3.6. Reconstructing Burdekin River Flow

October–September (i.e., annual) Burdekin River flow was estimated from the modern three-core average luminescence series using an exponential regression [*Isdale et al.*, 1998] model (Burdekin = –0.231 + exp ((0.437) + (4.324*coral))), 1972 to 2002. The modern luminescence series explained 93.4% of the variance in Burdekin River flow, 1972 to 2002. Given the reproducibility of the luminescence range in the mid-Holocene corals, this regression model was then used with the mid-Holocene four-core average luminescence series to reconstruct Burdekin River flow for Years 313 to 188 (NEL03 and NEL07) and Years 128–75, 67–0 from NEL01D. Additional regression models were tested based on (a) December–May Burdekin River flow and (b) summed "monthly" (from interpolation between annual luminescence minima) luminescence values for each year. These alternate models explained a similar amount of variance in the modern record and produced identical reconstructions for the mid-Holocene flow as for the October–September model.

3.7. Characteristics of Mid-Holocene Burdekin River Flow

The annual reconstructed Burdekin River flow for the two mid-Holocene windows shows substantially different characteristics to the modern record (Figure 6) and reconstructed flows during the Little Ice Age, 1631 to 1850 [*Lough*, 2007] (Table 5). Median flows in the mid-Holocene are about half of modern and interannual variability is about a third of modern values. The greatest difference is found in the lack of occurrence of flows $>8\,km^3$ in the mid-Holocene; such flows occur in ~40% of years in the 92 yearlong modern Burdekin record. Eighty percent of the 6.2 to 6.1 ka reconstructed annual flows were within the range 2.2 to 4.6 km^3 (Table 5), flows that do occur in the modern record but less frequently. Only 18% of years, 1922 to 2013, experienced flows typical of the mid-Holocene.

3.8. Intra-Annual Variability in the Mid-Holocene

Another feature of the mid-Holocene records, which differs from modern luminescence signatures, is the greater number of multiple (2 to 3) lines per year (Figure S8). For Years 294 to 234 of NEL03 and NEL07, there were 20 years (33%) when both colonies had ≥2 lines per year. For NEL01D, 30% of years had ≥lines per year. In the modern record, 1972 to 2002, only 2 years (6.5%) showed double annual lines in all three colonies, and none showed more than two lines. The more complex mid-Holocene signals were also evident from "monthly" luminescence for a 9 year window (Figure 7a) compared to the modern record (Figure 7b). The modern record was characterized by single annual peaks with only 1 year (1976–1977) with a double peak.

Table 4. Correlations Between Mid-Holocene Luminescence Indices for Four Cores From NEL03 and NEL07 Colonies and Four-Core Average Series, Years 294 to 234 (All Values Significant at 5% Level)

	NEL03A	NEL03D	NEL07B	NEL07C
NEL03A	1			
NEL03D	0.67	1		
NEL07B	0.66	0.68	1	
NEL07C	0.60	0.52	0.57	1
Four core	0.84	0.87	0.84	0.82

4. Discussion and Conclusions

We have developed proxy records of NE Queensland river flow from replicated luminescence records in modern and mid-Holocene massive *Porites* corals from Nelly Bay (~19°S, 147°E), Magnetic Island, in the central GBR. Gauged Burdekin River flow records, 1922–2013, show that 95% of the annual flow occurs from December to May in association with the summer

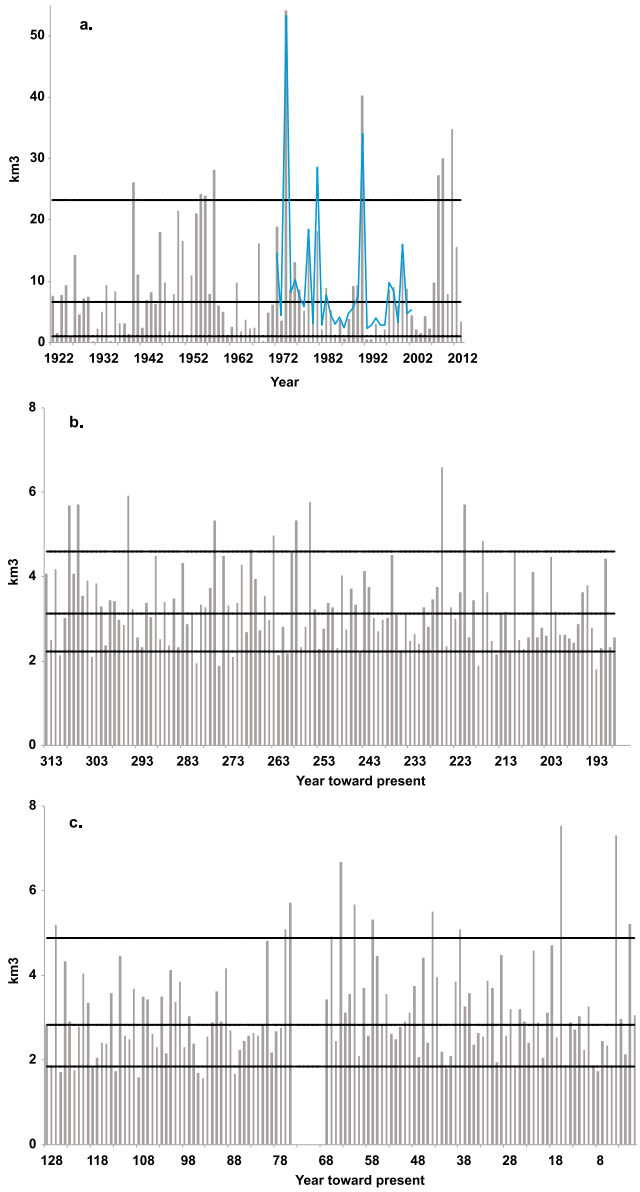

Figure 6. (a) Annual (October–September) Burdekin River flow, 1922 to 2013, and reconstructed flow, 1972 to 2002 (blue line); (b) reconstructed annual Burdekin River flow, Years 313 to 188, mid-Holocene 6.2 to 6.1 ka; and (c) reconstructed Burdekin River flow, Years 128 to 75, 67 to 0, mid-Holocene 6.0 to 5.9 ka. Dashed lines denote respective 90th percentile, median, and 10th percentile. Note different *y* axis scale for Figures 6b and 6c compared to Figure 6a.

Table 5. Observed (1922 to 2013), Reconstructed Little Ice Age (1631 to 1850) [*Lough*, 2007] and Reconstructed Mid-Holocene October–September Burdekin River Flow Characteristics (km^3)

	Observed 1922 to 2013	Reconstructed 1631 to 1850	Mid-Holocene 6.2 to 6.1 ka	Mid-Holocene 6.0 to 5.9 ka
Mean	9.1	10.7	3.3	3.1
% cv	104.4	59.9	29.9	37.7
Median	6.6	8.2	3.1	2.8
90th	23.2	21.4	4.6	4.9
10th	1.0	3.0	2.2	1.8
Range	22.2	18.4	2.4	3.0
n	92	220	126	122

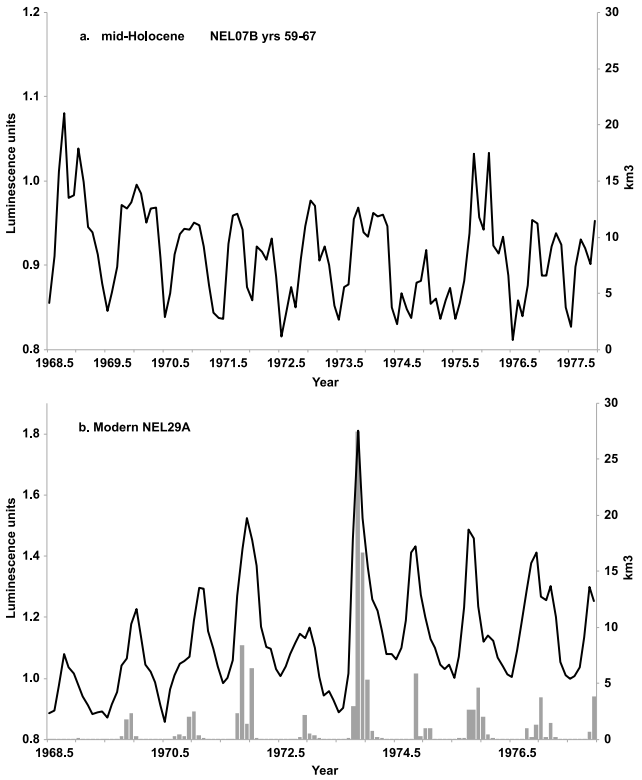

Figure 7. Comparison of "monthly" interpolated luminescence for (a) mid-Holocene NEL07B Years 255 to 247 and (b) modern NEL29A 1968 to 1978 and monthly Burdekin River flow (grey bars). (Note different *y* axis scale for mid-Holocene and modern corals).

monsoon. Median water year (October–September) flow is 6.62 km^3, but this shows substantial interannual variability from a maximum of 54.07 km^3 in 1973–1974 to a minimum of 0.25 km^3 in 1930–1931. The Burdekin River drains a large, ~130,000 km^2, catchment of the NE Queensland dry tropics, and hence, our reconstruction captures climate variability over a large part of NE tropical Queensland [*Lough*, 2007]. Seasonal and interannual variability of the Burdekin River also reflects summer monsoon rainfall over NE tropical Queensland which is significantly related to ENSO [*Lough*, 2011]. Here we examine whether the environment for coral growth in Nelly Bay, Burdekin River flow, and inferred NE Australian summer monsoon rainfall differed from present.

Before interpreting this record, we consider possible controls on the luminescence signal in the ~6 ka corals that could influence the reliability of our reconstructions. First, the location of the Burdekin River mouth has varied and in the mid-Holocene was either in its present position or ~50 km closer to Nelly Bay than present [*Fielding et al.*, 2006]. We would, therefore, expect, if mid-Holocene river flows were similar to present, that luminescence in the fossil Nelly Bay corals would be of similar magnitude to present or even more intense; this is in marked contrast to the observed difference. Second, relative sea level was ~1 to 1.5 m higher than present [*Lewis et al.*, 2013]. In the modern records a 1 m difference in depth does not significantly affect the magnitude of the luminescence signal (average luminescence range for NEL29A and NEL35A, which differ in depth by 1.4 m, was identical), unsurprising given the freshwater flood plumes can be 20 m thick [*King et al.*, 2001]. Third, diagenetic alteration is known to affect coral geochemical records [*McGregor and Abram*, 2008] but there is no evidence for secondary infilling in the mid-Holocene corals (Figures. S2 and S3). Fourth, we find no evidence that the luminescence signature due to humic acids [*Boto and Isdale*, 1985] differs between the mid-Holocene and present (Figure S4). Collectively, these various lines of evidence suggest that the luminescence records in the modern and mid-Holocene corals of Nelly Bay are comparable.

The growth characteristics (Figures S5 and S6) and calcification rates (Figure 3) of the mid-Holocene and modern corals are very similar. This implies that the mid-Holocene corals were growing in a similar nearshore, turbid environment as present-day Nelly Bay coral reefs. In addition, the average mid-Holocene calcification rate based

on three coral colonies suggests that the thermal environment (~25.9°C estimated from the Indo-Pacific *Porites* calcification versus SST relationship shown in Figure 3) was similar to the present (~26.1°C). This is also supported by an earlier SST reconstruction based on Sr/Ca ratios measured in two of the mid-Holocene corals, NEL03D and NEL01D [*Lewis*, 2005]. Although one coral record from the central GBR suggests SST were ~1°C warmer in the mid-Holocene [*Gagan et al*., 1998], several paleorecords for seas to the north and east of Australia suggest SST similar to present [*Gagan et al*., 2004; *Abram et al*., 2009; *Duprey et al*., 2012], as do multimodel PMIP2 ensembles [*Zhao and Harrison*, 2012; *Mantsis et al*., 2013], supporting the evidence that average annual SSTs at Nelly Bay are representative of the wider western Coral Sea and northern Australia (Figure S9).

Reconstructed Burdekin River flows at ~6 ka suggest that average flow was substantially lower (median ~ half of present) and less variable from year to year (Table 5 and Figure 6). Lower river flows and interannual variability suggest that the summer monsoon was weaker and modulation by ENSO reduced. Eastern Australian river flows are particularly sensitive to ENSO [*Ward et al*., 2010], and this is reflected in median Burdekin River flow being substantially different in El Niño (3.0 km^3, 20 events) and La Niña (9.4 km^3, 21 events) years, 1922 to 2013. Of the 18% of observed Burdekin River flows (1922 to 2013) with flows within the range of 80% of the mid-Holocene reconstruction (i.e., 2.2–4.6 km^3), 71% of these years were associated with neutral ENSO conditions. This again suggests reduced ENSO activity in the mid-Holocene. Caution is needed in interpreting relatively short paleoclimatic records in terms of ENSO variability as modeling studies indicate that there can be substantial modulation of ENSO characteristics on decadal and longer time scales [*Wittenberg*, 2009; *Borlace et al*., 2013]. Our two coral luminescence records suggest, however, that suppression of the NE Australian monsoon and potentially ENSO activity lasted at least ~300 years during the mid-Holocene.

Intra-annual variability of the luminescence signatures, as evidenced by multiple rather than a single annual luminescence peak, is more evident in the mid-Holocene than the modern corals (Figure 7). This could be evidence that intraseasonal monsoon variability, the Madden-Julian Oscillation (MJO) [*Wheeler et al*., 2009], was more evident at 6 ka than present; something hitherto unsuspected. Intriguingly, there is some evidence from the observational record that MJO variability is more apparent during weak monsoon seasons [*Hendon et al*., 1999]. The inferred record of MJO variability may explain the apparently moist conditions and greater vegetation cover in tropical Australia during the mid-Holocene [*Donders et al*., 2007; *Mooney et al*., 2011]. Although the magnitude of Burdekin flow appears to have been significantly lower than present, we suggest delivery of frequent, low-intensity rainfall may have been more effective at sustaining terrestrial vegetation; something not possible to identify in low-resolution records from the region. Our annually resolved, absolutely dated window of river flow therefore provides a unique insight into the climate dynamics across NE Queensland and the western Coral Sea, a region currently influenced by the northern Australian summer monsoon, with ENSO modulating interannual and the MJO modulating intra-annual rainfall variability [*Risbey et al*., 2009]. Our coral records indicate that ~6 ka thermal conditions off NE Australia were similar to present but that the summer monsoon was weaker and interannual ENSO variability was suppressed allowing the intraseasonal variability of the MJO to be more evident.

Acknowledgments

We thank Harry Hendon for his insights into the MJO and Eric Matson for his skilled technical support. We also acknowledge the late Bruce Parker, Monty Devereux, Curtain Bros. Pty. Ltd., and 10 Force Support Battalion who helped retrieve the mid-Holocene corals from Nelly Bay for AIMS. This work was supported by the Australian Institute of Marine Science and Australian Research Council (FL100100195). The Burdekin River reconstructions are lodged with AIMS Data Centre and the NOAA Paleoclimatology Data Center. J.M.L. conceived the study, undertook the luminescence and growth analyses, and wrote the initial manuscript. L.E.L. carried out the comparison of modern and Holocene luminescence characteristics. S.E.L. undertook geochemical and diagenetic analyses of the mid-Holocene corals. C.S.M.T., J.G.P., C.G.C., and A.G.H. undertook ^{14}C dating and interpretation. All authors contributed to writing the paper and interpreting the results.

References

Abram, N. J., H. V. McGregor, M. K. Gagan, W. S. Hantoro, and B. W. Suwargadi (2009), Oscillations in the southern extent of the Indo-Pacific warm pool during the mid-Holocene, *Quat. Sci. Rev.*, *28*, 2794–2803, doi:10.1016/j.quascirev.2009.07.006.

Barnes, D. J., R. B. Taylor, and J. M. Lough (2003), Measurement of luminescence in coral skeletons, *J. Exp. Mar. Biol. Ecol.*, *295*, 91–106.

Borlace, S., W. Cai, and A. Santoso (2013), Multidecadal ENSO amplitude variability in a 1000-year simulation of a coupled global climate model: Implication for observed ENSO variability, *J. Clim.*, *26*, 9399–9407, doi:10.1175/JCLI-D-13-00281.1.

Boto, K., and P. Isdale (1985), Fluorescent bands in massive corals result from terrestrial fulvic acid inputs to nearshore zone, *Nature*, *315*, 396–397.

Braconnot, P., et al. (2007), Results of PMIP2 coupled simulations of the Mid-Holocene and Last Glacial Maximum—Part 1: experiments and large-scale features, *Clim. Past*, *3*, 261–277, doi:10.5194/cp-3-261-2007.

Braconnot, P., Y. Luan, S. Brewer, and W. Zheng (2012a), Impact of Earth's orbit and freshwater fluxes on Holocene climate mean seasonal cycle and ENSO characteristics, *Clim. Dyn.*, *38*, 1081–1092, doi:10.1007/s00382-011-1029-x.

Braconnot, P., S. P. Harrison, M. Kageyama, P. J. Bartlein, V. Masson-Delmotte, A. Abe-Ouchi, B. Otto-Bliesner, and Y. Zhao (2012b), Evaluation of climate models using palaeoclimate data, *Nat. Clim. Change*, doi:10.1038/NCLIMATE1456.

Bronk Ramsey, C. (2008), Radiocarbon dating: Revolutions in understanding, *Archaeometry*, *50*, 249–275, doi:10.1111/j.1475-4754.2008.00394.x.

Bronk Ramsey, C., and S. Lee (2013), Recent and planned developments of the program OxCal, *Radiocarbon*, *55*, 720–730, doi:10.2458/azu_js_rc.55.16215.

Brown, J., A. W. Tudhope, M. Collins, and H. V. McGregor (2008), Mid-Holocene ENSO: Issues in quantitative model-proxy data comparisons, *Paleoceanography*, *23*, PA3202, doi:10.1029/2007PA001512.

Bureau of Meteorology (2012), *Record-Breaking La Niña Events*, pp. 28 , Bureau of Meteorology, Melbourne, Australia.

Cane, M. A. (2005), The evolution of El Niño, past and future, *Earth Planet. Sci. Lett.*, *230*, 227–240, doi:10.1016/j.epsl.2004.12.003.

Clement, A. C., R. Seager, and M. A. Cane (2000), Suppression of El Niño during the mid-Holocene by changes in the Earth's orbit, *Paleoceanography*, *15*, 731–737, doi:10.1029/1999PA000466.
Cobb, K. M., N. Westphal, H. R. Sayani, J. T. Watson, E. Di Lorenzo, H. Cheng, R. L. Edwards, and C. D. Charles (2013), Highly variable El Niño-Southern Oscillation throughout the Holocene, *Science*, *339*, 67–70, doi:10.1126/science.1228246.
Collins, M., et al. (2010), The impact of global warming on the tropical Pacific Ocean and El Niño, *Nat. Geosci.*, *3*, 391–397, doi:10.1038/ngeo868.
Conroy, J. L., J. T. Overpeck, J. E. Cole, T. M. Shanahan, and M. Steinitz-Kannan (2008), Holocene changes in eastern tropical Pacific climate inferred from a Galápagos lake sediment record, *Quat. Sci. Rev.*, *27*, 1166–1180, doi:10.1016/j.quascirev.2008.02.015.
Donders, T. H., S. G. Haberle, G. Hope, F. Wagner, and H. Visscher (2007), Pollen evidence for the transition of the Eastern Australian climate system from the post-glacial to the present-day ENSO mode, *Quat. Sci. Rev.*, *26*, 1621–1637, doi:10.1016/j.quascirev.2006.11.018.
Duprey, N., C. E. Lazareth, T. Corrège, F. Le Cornec, C. Maes, N. Pujol, M. Madeng-Yogo, S. Caquineau, C. Soares Derome, and G. Cabioch (2012), Early mid-Holocene SST variability and surface-ocean water balance in the southwest Pacific, *Paleoceanography*, *27*, PA4207, doi:10.1029/2012PA002350.
Enmar, R., M. Stein, M. Bar-Matthews, E. Sass, A. Katz, and B. Lazar (2000), Diagenesis in live corals from the Gulf of Aqaba. I. The effect on paleo-oceanography tracers, *Geochim. Cosmochim. Acta*, *64*, 3123–3132, doi:10.1016/S0016-7037(00)00417-8.
Fang, L.-S., and Y.-C. Chou (1992), Concentration of fulvic acid in the growth bands of hermatypic corals in relation to local precipitation, *Coral Reefs*, *11*, 187–191.
Fielding, C. R., J. D. Trueman, and J. Alexander (2006), Holocene depositional history of the Burdekin River delta of northeastern Australia: A model for a low-accommodation, highstand delta, *J. Sed. Res.*, *76*, 411–428, doi:10.2110/jsr.2006.032.
Finlayson, B. L., and T. A. McMahon (1988), Australia v. the world: A comparative analysis of streamflow characteristics, in *Fluvial Geomorphology of Australia*, edited by R.F. Warner, pp. 17–40, Academic Press, Sydney, Australia.
Gagan, M. K., L. K. Ayliffe, D. Hopley, J. A. Cali, G. E. Mortimer, J. Chappell, M. T. McCulloch, and M. J. Head (1998), Temperature and surface-ocean water balance of the mid-Holocene tropical western Pacific, *Science*, *279*, 1014–1018.
Gagan, M. K., E. J. Hendy, S. G. Haberle, and W. S. Hantoro (2004), Post-glacial evolution of the Indo-Pacific warm pool and El Niño-Southern Oscillation, *Quaternary Int.*, *118-119*, 127–143, doi:10.1016/S1040-6182(03)00134-4.
Griffiths, M. L., et al. (2009), Increasing Australian-Indonesian monsoon rainfall linked to early Holocene sea-level rise, *Nat. Geosci.*, *2*, 636–639, doi:10.1038/ngeo605.
Grove, C. A., R. Nagtegall, J. Zinke, T. Scheufen, B. Koster, S. Kasper, M. T. McCulloch, G. van den Bergh, and G.-J. A. Brummer (2010), River runoff reconstructions from novel spectral luminescence scanning in massive coral skeletons, *Coral Reefs*, *29*, 579–591, doi:10.1007/s00338-010-0629-y.
Grove, C. A., J. Zinke, F. Peeters, W. Park, T. Scheufen, S. Kasper, B. Randriamanantsoa, M. T. McCulloch, and G.-J. A. Brummer (2013), Madagascar corals reveal a multidecadal signature of rainfall and river runoff since 1708, *Clim. Past*, *9*, 641–656, doi:10.5194/cp-9-641-2013.
Haberle, S. G. (2005), A 23,000-yr pollen record from Lake Euramoo, wet tropics of NE Queensland, Australia, *Quat. Res.*, *64*, 343–356, doi:10.1016/j.yqres.2005.08.013.
Harrison, S. P., P. Braconnot, S. Joussaume, C. Hewitt, and R. J. Stouffer (2002), Fourth international workshop of the Palaeoclimate Modelling Intercomparison Project (PMIP): Launching PMIP Phase II, *Eos Trans. AGU*, *83*, 447, doi:10.1029/2002EO000317.
Hendon, H. H., C. Zhang, and J. D. Glick (1999), Interannual variation of the Madden-Julian Oscillation during austral summer, *J. Clim.*, *12*, 2538–2550, doi:10.175/1520-0442(1999)012<2538:IVOTMJ>2.0.CO:2.
Hendy, E. J., M. K. Gagan, and J. M. Lough (2003), Chronological control of coral records using luminescent lines and evidence for non-stationary ENSO teleconnections in northeast Australia, *The Holocene*, *13*, 187–199, doi:10.1191/0959683603hi606rp.
Hendy, E. J., M. K. Gagan, J. M. Lough, M. McCulloch, and P. B. deMenocal (2007), Impact of skeletal dissolution and secondary aragonite on trace element and isotopic climate proxies in *Porites* corals, *Paleoceanography*, *22*, PA4101, doi:10.1029/2007/PA001462.
Ingalls, A. E., C. Lee, and E. R. M. Druffel (2003), Preservation of organic matter in mound-forming coral skeletons, *Geochim. Cosmochim. Acta*, *67*, 2827–2841, doi:10.1016/S0016-7037(03)00079-6.
Isdale, P. J. (1984), Fluorescent bands in massive corals record centuries of coastal rainfall, *Nature*, *310*, 578–579.
Isdale, P. J., and E. Daniel (1989), The design and deployment of a new lightweight submarine fixed drilling system for the acquisition and preparation of coral cores, *Mar. Technol. Soc. J.*, *23*, 3–8.
Isdale, P. J., B. J. Stewart, K. S. Tickle, and J. M. Lough (1998), Palaeohydrological variation in a tropical river catchment: A reconstruction using fluorescent bands in corals of the Great Barrier Reef, Australia, *The Holocene*, *8*, 1–8, doi:10.119/095968398670905088.
Jupiter, S., G. Roff, G. Marion, M. Henderson, V. Schrameyer, M. McCulloch, and O. Hoegh-Guldberg (2008), Linkages between coral assemblages and coral proxies of terrestrial exposure along a cross-shelf gradient on the southern Great Barrier Reef, *Coral Reefs*, *27*, 887–903, doi:10.1007/s00338-008-0422-3.
Kiem, A. S., S. W. Franks, and G. Kuezera (2003), Multidecadal variability of flood risk, *Geophys. Res. Lett.*, *30*(2), 1035, doi:10.1029/2002GL015992.
King, B., F. McAllister, E. Wolanski, T. Done, and S. Spagnol (2001), River plume dynamics in the central Great Barrier Reef, in *Oceanographic Processes of Coral Reefs: Physical and Biological Links in the Great Barrier Reef*, edited by E. Wolanski, pp. 145–159, CRC Press, Boca Raton, Fla.
Klein, R., Y. Loya, G. Gvirtzman, P. J. Isdale, and M. Susic (1990), Seasonal rainfall in the Sinai Desert during the late Quaternary inferred from fluorescent bands in fossil corals, *Nature*, *345*, 145–147.
Koutavas, A., and S. Joanides (2012), El Niño-Southern Oscillation extrema in the Holocene and Last Glacial Maximum, *Paleoceanography*, *27*, PA4208, doi:10.1029/2012PA002378.
Lewis, S. E. (2005), Environmental trends in the GBR lagoon and Burdekin River catchment during the mid-Holocene and since European settlement using *Porites* coral records, Magnetic Island, Queensland, PhD thesis, School of Earth and Environmental Sciences, James Cook Univ., Townsville, Australia.
Lewis, S. E., J. E. Brodie, M. T. McCulloch, J. Mallela, S. D. Jupiter, H. Stuart Williams, J. M. Lough, and E. G. Matson (2012), An assessment of an environmental gradient using coral geochemical records, Whitsunday Islands, Great Barrier Reef, Australia, *Mar. Poll. Bull.*, *65*, 396–319, doi:10.1016/j.marpolbul.2011.09.030.
Lewis, S. E., C. R. Sloss, C. V. Murray-Wallace, C. D. Woodroffe, and S. G. Smithers (2013), Post-glacial sea-level changes around the Australian margin: A review, *Quat. Sci. Rev.*, *74*, 115–138, doi:10.1016/j.quascirev.2012.09.006.
Liu, Z., S. P. Harrison, J. Kutzbach, and B. Otto-Bliesner (2004), Global monsoons in the mid-Holocene and oceanic feedback, *Clim. Dyn.*, *22*, 157–182, doi:10.1007/s00382-003-0372-y.
Llewellyn, L. E., Y. L. Everingham, and J. M. Lough (2012), Pharmacokinetic modelling of multi-decadal luminescence time series in coral skeletons, *Geochim. Cosmochim. Acta*, *83*, 263–271, doi:10.1016/j.gca.2011.12.028.
Lough, J. M. (1991), Rainfall variations in Queensland, Australia: 1891–1986, *Int. J. Climatol.*, *11*, 745–768.
Lough, J. M. (1994), Climate variation and El Niño-Southern Oscillation events on the Great Barrier Reef, *Coral Reefs*, *13*, 181–195.
Lough, J. M. (2007), Tropical river flow and rainfall reconstructions from coral luminescence: Great Barrier Reef, Australia, *Paleoceanography*, *22*, PA2218, doi:10.1029/2006PA001377.

Lough, J. M. (2008), Coral calcification from skeletal records revisited, *Mar. Ecol. Prog. Ser.*, *373*, 257–264, doi:10.3354/meps07398.
Lough, J. M. (2011), Great Barrier Reef coral luminescence reveals rainfall variability over northeastern Australia since the 17th century, *Paleoceanography*, *26*, PA2201, doi:10.1029/2010PA002050.
Lough, J. M., and D. J. Barnes (2000), Environmental controls on growth of the massive coral *Porites*, *J. Exp. Mar. Biol. Ecol.*, *245*, 225–243, doi:10.1016/S0022-098(99)00168-9.
Lough, J. M., and T. F. Cooper (2011), New insights from coral growth band studies in an era of rapid environmental change, *Earth Sci. Rev.*, *108*, 170–184, doi:10.1016/j.earscirev.2011.07.001.
Lough, J. M., D. J. Barnes, M. J. Devereux, B. J. Tobin, and S. Tobin (1999), Variability in growth characteristics of massive Porites on the Great Barrier Reef, CRC Reef Research Centre Technical Report No. 28, Townsville, CRC Reef Research Centre, 95 pp.
Lough, J. M., D. J. Barnes, and F. A. McAllister (2002), Luminescent lines in corals from the Great Barrier Reef provide spatial and temporal records of reefs affected by land runoff, *Coral Reefs*, *21*, 333–343, doi:10.1007/s00338-002-0253-6.
Luan, Y., P. Braconnot, Y. Yu, W. Zheng, and O. Marti (2012), Early and mid-Holocene climate in the tropical Pacific: Seasonal cycle and interannual variability induced by insolation changes, *Clim. Past*, *8*, 1093–1108, doi:10.5194/cp-8-1093-2012.
Mantsis, D. F., B. R. Lintner, A. J. Broccoli, and M. Khodri (2013), Mechanisms of mid-Holocene precipitation change in the South Pacific Convergence Zone, *J. Clim.*, *26*, 6937–6953, doi:10.1175/JCLI-D-12-00684.1.
Mantua, N. J., S. R. Hare, Y. Zhang, J. M. Wallace, and R. C. Franks (1999), A Pacific interdecadal oscillation with impacts on salmon production, *Bull. Am. Meteorol. Soc.*, *78*, 1069–1079, doi:10.1175/1520-0477(1997)078<1069:APICOW>2.0.CO:2.
McBride, J. L. (1987), The Australian summer monsoon, in *Monsoon Meteorology*, edited by C.-P. Chang and T. N. Krishnamurti, pp. 203–231, Oxford Univ. Press, Oxford.
McGregor, H. V., and N. J. Abram (2008), Images of diagenetic textures in *Porites* from Papua New Guinea and Indonesia, *Geochem. Geophys. Geosyst.*, *9*, Q10013, doi:10.1029/2008GC002093.
McGregor, H. V., and M. K. Gagan (2003), Diagenesis and geochemistry of Porites corals from Papua New Guinea: Implications for paleoclimate reconstruction, *Geochim. Cosmochim. Acta*, *67*, 2147–2156, doi:10.106/S0016-7037(02)01050-5.
McGregor, H. V., and M. K. Gagan (2004), Western Pacific $\delta^{18}O$ records of anomalous Holocene variability in the El Niño-Southern Oscillation, *Geophys. Res. Lett.*, *31*, L11204, doi:10.1029/2004GL019972.
McGregor, H. V., M. J. Fischer, M. K. Gagan, D. Fink, S. J. Phipps, H. Wong, and C. D. Woodroffe (2013), A weak El Niño/Southern Oscillation with delayed seasonal growth around 4,300 years ago, *Nat. Geosci.*, *6*, doi:101038/ngeo1936.
Meinke, H., P. de Voil, G. L. Hammer, S. Power, R. Allan, R. G. Stone, C. Folland, and A. Poigieter (2005), Rainfall variability at decadal and longer time scales: Signal or noise?, *J. Clim.*, *18*, 89–96, doi:10.1175/jcli-3263.1.
Mooney, S. D., et al. (2011), Late Quaternary fire regimes of Australasia, *Quat. Sci. Rev.*, *30*, 28–46, doi:10.1016/j.quascirev.2010.10.010.
Moses, C. S., and P. K. Swart (2006), Stable isotope and growth records in corals from the island of Tobago: Not simply a record of the Orinoco, in *Proceedings of 10th International Coral Reef Symposium*, Okinawa, pp. 580–587.
Moy, C. M., G. O. Seltzer, D. T. Rodbell, and D. M. Anderson (2002), Variability of El Niño/Southern Oscillation activity at millennial timescales during the Holocene epoch, *Nature*, *420*, 162–165.
Müller, A., M. K. Gagan, and M. T. McCulloch (2001), Early marine diagenesis in corals and geochemical consequences for paleoceanographic reconstructions, *Geophys. Res. Lett.*, *28*, 4471–4474, doi:10.1029/2001GL013577.
Nagtegaal, R., C. A. Grove, S. Kasper, J. Zinke, W. Boer, and G.-J. A. Brummer (2012), Spectral luminescence and geochemistry of coral aragonite: Effects of whole-core treatment, *Chem. Geol.*, *318–319*, 6–15, doi:10.1016/j.chemgeo.2012.05.006.
Peng, Z., X. He, Z. Zhang, J. Zhou, L. Sheng, and H. Gao (2002), Correlation of coral fluorescence with nearshore rainfall and runoff in Hainan Island, South China Sea, *Prog. Nat. Sci.*, *12*, 41–44.
Power, S., T. Casey, C. Folland, A. Colman, and V. Mehta (1999), Interdecadal modulation of the impact of ENSO on Australia, *Clim. Dyn.*, *15*, 319–342.
Reimer, P., et al. (2013), IntCal13 and Marine13 radiocarbon age calibration curves 0–50,000 years cal BP, *Radiocarbon*, *55*, 1869–1887, doi:10.2458/azu_js_rc.55.16947.
Risbey, J. S., M. J. Pook, P. C. McIntosh, M. C. Wheeler, and H. H. Hendon (2009), On the remote drivers of rainfall variability in Australia, *Mon. Weather Rev.*, *137*, 3233–3253, doi:10.1175/2009MWR2861.1.
Roberts, W., D. Battisti, and A. Tudhope (2013), ENSO in the mid-Holocene according to CSM and HadCM3, *J. Clim.*, doi:10.1175/JCLI-D-13-00251.1.
Schulmeister, J., D. T. Rodbell, M. K. Gagan, and G. O. Seltzer (2006), Inter-hemispheric linkages in climate change: Paleo-perspectives for future climate change, *Clim. Past*, *2*, 167–185, doi:10.5194/cp-2-167-2006.
Scoffin, T. P., A. W. Tudhope, and B. E. Brown (1989), Fluorescent and skeletal density banding in *Porites lutea* from Papua New Guinea and Indonesia, *Coral Reefs*, *7*, 169–178.
Smith, T. J., J. H. Hudson, M. B. Roblee, G. V. N. Powell, and P. J. Isdale (1989), Freshwater flow from the everglades to Florida Bay: A historical reconstruction based on fluorescence banding in the coral *Solenastrea bournoni*, *Bull. Mar. Sci.*, *44*, 274–282.
Tudhope, A. W., D. W. Lea, G. B. Shimmield, C. P. Chilcott, and S. Head (1996), Monsoon climate and Arabian Sea coastal upwelling recorded in massive corals from southern Oman, *Palaios*, *11*, 347–361.
Tudhope, A. W., C. P. Chilcott, M. T. McCulloch, E. R. Cook, J. Chappell, R. M. Ellam, D. W. Lea, J. M. Lough, and G. B. Shimmield (2001), Variability in the El Niño-Southern Oscillation through a glacial-interglacial cycle, *Science*, *291*, 1511–1517, doi:10.1126/science.1057969.
Verdon, D. C., A. M. Wyatt, A. S. Kiem, and S. W. Franks (2004), Multi-decadal variability of rainfall and streamflow: Eastern Australia, *Water Resour. Res.*, *40*, W10201, doi:10.1029/2004WR003234.
Wanner, H., et al. (2008), Mid- to late Holocene climate change: An overview, *Quat. Sci. Rev.*, *27*, 1791–1828, doi:10.1016/j.quascirev.2008.06.013.
Ward, P. J., W. Beets, L. M. Bouwer, J. C. J. H. Aerts, and H. Renssen (2010), Sensitivity of river discharge to ENSO, *Geophys. Res. Lett.*, *37*, L12402, doi:10.1029/2010GL043215.
Wheeler, M. C., H. H. Hendon, S. Cleland, H. Meinke, and A. Donald (2009), Impacts of the Madden-Julian Oscillation on Australian rainfall and circulation, *J. Clim.*, *22*, 1482–1498, doi:10.1175/2008JCLI2595.1.
Wittenberg, A. T. (2009), Are historical records sufficient to constrain ENSO simulations?, *Geophys. Res. Lett.*, *36*, L12702, doi:10.1029/2009GL038710.
Zhao, Y., and S. P. Harrison (2012), Mid-Holocene monsoons: A multi-model analysis of the interhemispheric differences in the responses to orbital forcing and ocean feedbacks, *Clim. Dyn.*, *39*, 1457–1487, doi:10.1007/s00382-011-1103-z.
Zheng, W., P. Braconnot, E. Guilyardi, U. Merkel, and Y. Yu (2008), ENSO at 6 ka and 21 ka from ocean-atmosphere coupled model simulations, *Clim. Dyn.*, *30*, 745–762, doi:10.1007/s00382-007-0320-3.